Intensity Modulated Photocurrent Spectroscopy for solar energy conversion devices. What does negative value mean?

Small perturbation techniques constitute a wide family of tools for the characterization of solar energy conversion devices such as photovoltaic cells and photoelectrochemical (PEC) cells for solar fuel production. Two main small perturbation methods frequently used in the area of solar energy conversion materials are Impedance Spectroscopy (IS) and Intensity Modulated Photocurrent Spectroscopy (IMPS). The first one consists of applying a small voltage perturbation and measuring modulated extracted current. The second one consists of applying the perturbation to the illumination and measuring the modulated extracted current.

It is well known that we can get the resistances and the capacitances of the system from the real and the imaginary part of the IS spectra respectively, and recently we have demonstrated that the differential External Quantum Efficiency (EQE_{diff}) can be obtained from the real part of the IMPS spectra.[1] However, researchers working on solar cell characterization such as the IS of metal halide perovskite solar cells are well aware that spectral responses are often not straightforward to interpret. There appear frequently experimental responses that display exotic behaviours that do not correspond to usual quantities or phenomena. For example, in the case of IS, there have been reports about *negative* values of the real part of the impedance, which are associated to negative resistances.[2] Negative values of the IS imaginary part or negative capacitances have been also reported, particularly in recent results on perovskite solar cells.[3-7] Those unexpected results, as compared to ordinary physical-chemical behaviour, are difficult to explain and their origins are still under debate, with different interpretations found in the literature.[6-9]

Recently, IMPS has become increasingly popular for understanding the charge transfer/transport/recombination dynamics and its connection to performance limitations of semiconductor materials in PECs.[10-17] One such material is $BiVO_4$, which has become an attractive candidate as a photoanode for water oxidation in PEC water splitting cells, due to its suitable band gap and valence band position for light absorption and hole injection, respectively.[18-20] Despite these desirable properties, this material also exhibits several limitations related to the charge mobility within the bulk, concomitant to surface limitations evidenced as a low charge injection efficiency.[19] In particular, the origin of these surface limitations has been extensively discussed, leading to divergent interpretations on whether the bare surface of $BiVO_4$ is catalytically active or not, and hence, about the true role of the co-catalysts used to improve the photoelectrode performance.[15, 21-22] This context motivates the investigation of the intrinsic and surface properties of this promising material in order to overcome its current limitations and, furthermore, to properly understand and interpret the results obtained from small perturbation experimental techniques.

In this Viewpoint we handle a puzzling result that is frequently obtained in IMPS measurements, particularly when measuring photoanodes for water splitting applications. It has been observed that at the region of applied potential close to the open-circuit potential (OCP), the IMPS response goes to the *negative* real part of the complex plane representation at low frequency. This phenomenon is usually accompanied by a photocurrent sign switching, observed in linear sweep voltammetry (LSV) measurements. This feature has been reported in $BiVO_4$ photoanodes,[23] for inject-printed $CuBi_2O_4$ photocathodes[24] and in Gold- decorated Cadmium chalcogenide nanorods.[25]

While the switch of the sign of the low frequency value of the IMPS response, $Q(0)$, that reaches *negative* values under different conditions, has been associated to the sign of the photocurrent in many papers,[23-25] here we show that such interpretation is not consistent with the experimental measurements. A physical model based on the general features of IMPS[1] will be presented to explain negative $Q(0)$, that sheds new light into the interpretation of quantum efficiency and charge extraction in solar energy conversion devices.

The two techniques of IS and IMPS can be summarized in a general expression that relates the photocurrent, $\hat{j}_e$, arising from a small perturbation of light, $\hat{j}_\phi$, or voltage, $\hat{V}$, at any frequency as a linear combination of the IMPS (Q) and IS (Z) transfer functions expressed as coefficients:[26]

$$\hat{j}_e = Q(\omega)\hat{j}_\phi + Z^{-1}(\omega)\hat{V} \tag{1}$$

From this general constraint, the IS response is obtained in the absence of modulated illumination ($\hat{j_\phi} = 0$) and otherwise IMPS when $\hat{V} = 0$. IS combines current and voltage, and consequently, the real part of the transfer function is related to a resistance and the imaginary part conveys information about capacitance. Therefore, IS enables distinguishing between loss processes (resistive) and polarizing processes (capacitive) and it provides an estimation of the time-scale for these processes. Moreover, the low frequency intercept corresponds to the DC resistance:

$$Z(0) = \frac{\hat{V}(0)}{\hat{j_e}(0)} = \frac{\partial \bar{V}}{\partial \overline{j_e}} = R_{DC} \tag{2}$$

where $\bar{V}$ and $\overline{j_e}$ are the DC voltage and steady state extracted current respectively. On the other hand, IMPS relates the extracted photocurrent and the illumination, as shown in the scheme of **Figure 1a.** Therefore, the real part of its transfer function is related to the variation of the EQE.

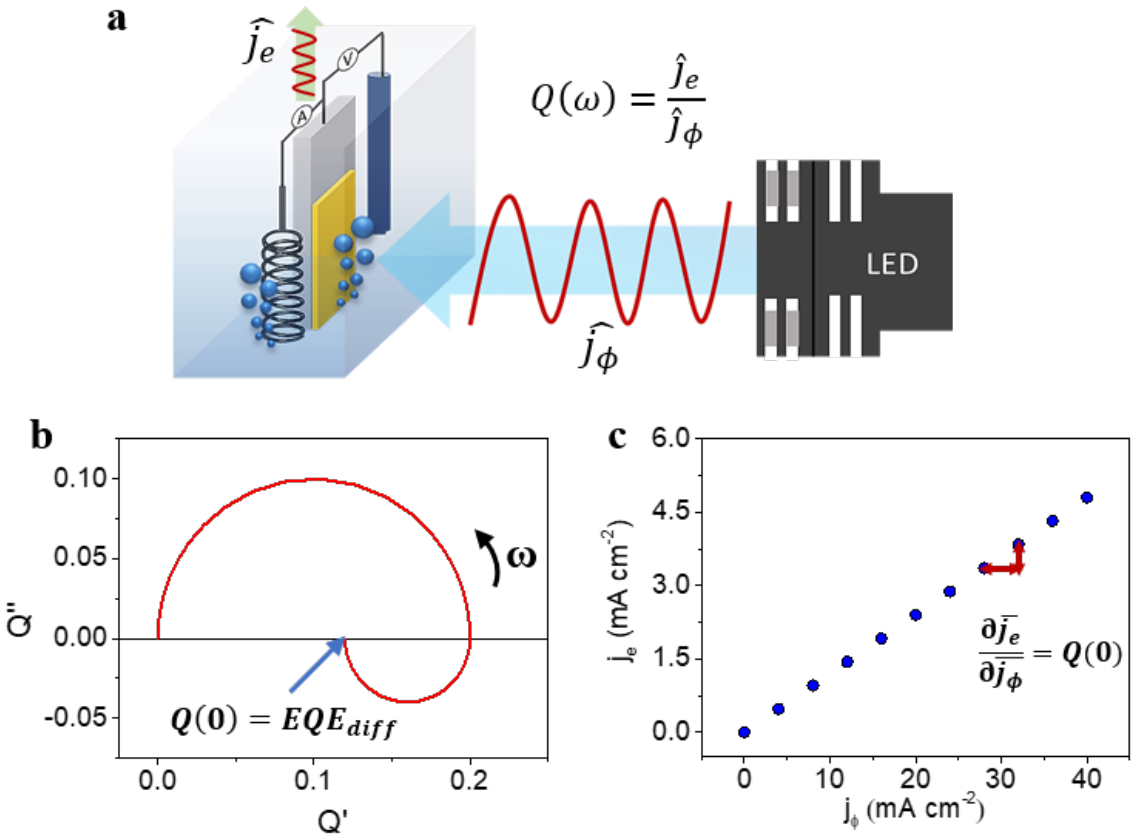

Figure 1. a Schematic representation of IMPS measurement setup in solar conversion photoelectrodes; **b** IMPS complex representation, where Q' and $-Q''$ are the real and imaginary components, respectively, of the transfer function $Q(\omega)$; **c** Representative $j_e - j_\phi$ plot showing that the slope in this graph is directly linked whit the $Q(0)$ intercept from IMPS measurements.

Similarly to IS and the R_{DC}, the low frequency value of the IMPS is directly linked with the DC component of the slope of $\bar{j_e}$ with $\bar{j_\phi}$, as depicted in **Figure 1c**.[27]

$$Q(0) = \frac{\hat{j_e}(0)}{\hat{j_\phi}(0)} = \frac{\partial \bar{j_e}}{\partial \bar{j_\phi}} \tag{3}$$

This expression has a connection with the external quantum efficiency (EQE), which is a key parameter for the evaluation of solar conversion devices, including PECs, since it gives the ratio of the incident photons that are converted into electron-hole pairs further extracted, as function of the wavelength. Usually, in photoelectrochemical characterization, the EQE is referred as the Incident Photon-to-Current Efficiency (IPCE) which is calculated by measuring the extracted steady state photocurrent $\bar{j_e}$ under a monochromatic light source of DC spectral photon flux, $\bar{\Phi}(\lambda)$. We will refer to this quantity as EQE_{SS}, defined as:

$$EQE_{SS} = \frac{j_{ph}}{q\phi_{ph}} = \frac{\bar{j}_e}{\bar{j}_\phi} \tag{4}$$

Here, q is the elementary charge. However, another method widely employed in solar conversion device characterization involves the measurement of the differential spectral response, EQE_{diff}.[28] In this method, the sample is illuminated by a DC white light intensity, and the extracted photocurrent is measured under a small low frequency perturbation of monochromatic light. Usually, an optical chopper is employed to provide the AC perturbation. At infinitely slow perturbation, i.e. $\omega \to 0$, the EQE_{diff} can be written as:

$$EQE_{diff} = \frac{\hat{j}_e}{\hat{j}_\phi}(\omega \to 0) \approx \frac{\partial \overline{j_e}}{\partial \overline{j_\phi}} \quad (5)$$

Comparing equations (3) and (5) we get that:

$$Q(0) = EQE_{diff} \quad (6)$$

Hence, the IMPS measurements constitute an alternative method to obtain the EQE_{diff}, and it must match the slope of the extracted photocurrent with changing the illumination, as already shown by Ravishankar et al.[28]

Based on these definitions, we show that the IMPS transfer function negative value is associated to the derivative of the photocurrent with the illumination independently whether the photocurrent is positive or negative. To demonstrate this statement, we show an example of negative $Q(0)$ and negative EQE_{diff}, and simultaneously, positive value of its photocurrent. Moreover, we demonstrate experimentally the match of values of $Q(0)$ and EQE_{diff} as predicted by Eq. (6).

Figure 2a shows a linear sweep voltammetry (LSV) curve performed on a $BiVO_4$ photoanode, at monochromatic DC illumination (λ =470 nm; 90 mW cm^{-2}) and scan rate of 50 mV s^{-1}. The complete details about the photoelectrode preparation and the experimental setup can be found in the **Supporting Information** file. The inset in **Figure 2a** shows the region closer to the OCP, which is around 0.25 V vs RHE. Below this value, negative photocurrent is obtained, leading to a photocurrent switching point, and such photocurrent is strongly dependent on the incident light intensity. Similar behaviour has been previously reported on $BiVO_4$ photoanodes.[23]

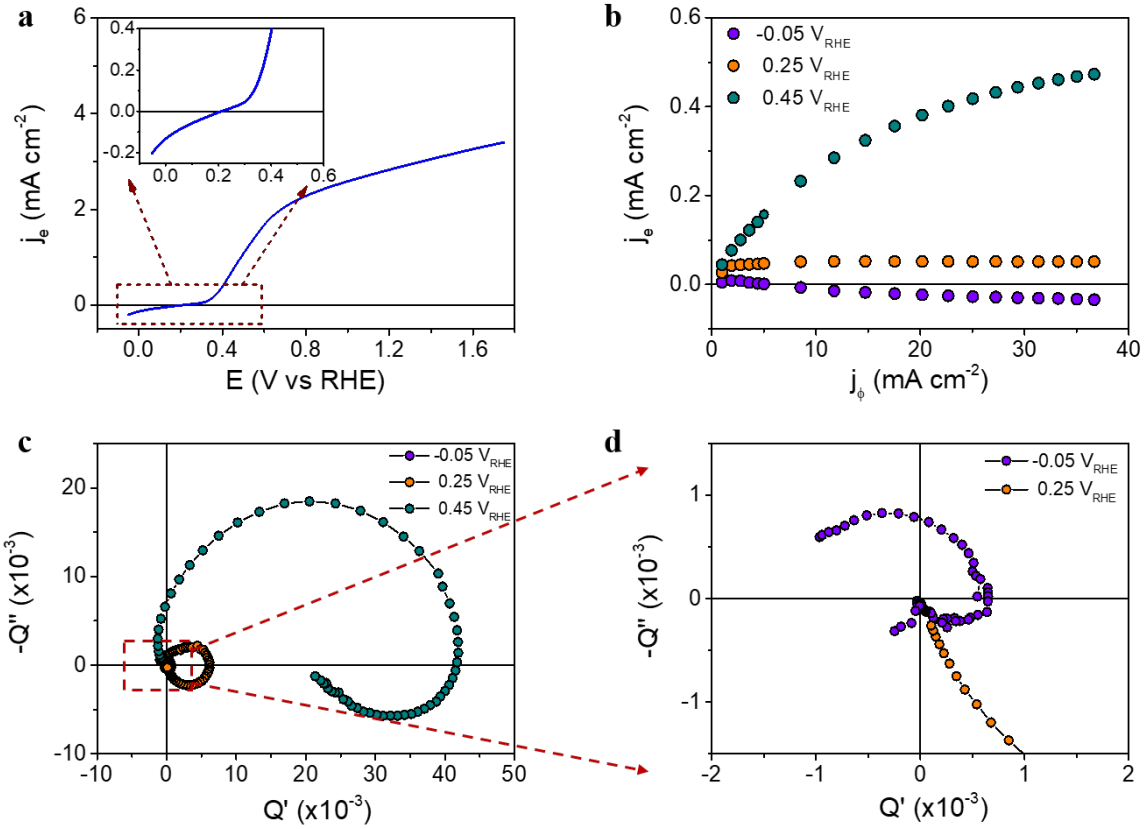

Figure 2. a Linear sweep voltammetry for a $BiVO_4$ photoanode, recorded at 50 mV s^{-1} under monochromatic DC illumination (λ=470 nm, 90 mW cm^{-2}). The inset shows the region closer to the OCP value; **b** $j_e - j_\phi$ plot at representative applied potentials closer to the OCP value; **c** Q complex representation measured at j_ϕ=36 mA cm^{-2} (corresponding to 90 mW cm^{-2}) at different applied potentials; **d** Magnification of region of **c**. All the measurements were performed in potassium phosphate buffer, at pH 7.5.

In **Figure 2b**, we show the relationship between the steady state extracted photocurrent and the incident light intensity at representative applied potentials. At applied potentials above the OCP, the extracted photocurrent tends to increase with increased photon flux, however this trend is nonlinear, and the slope tends to decrease with increasing light intensity. This means that the EQE_{diff} decreases with light intensity. At closer values to the OCP, the extracted current does not significantly change with light intensity, then the EQE_{diff} is zero. This situation changes at potentials below the OCP, where the extracted photocurrent becomes more negative when increasing the photon flux, meaning that the differential EQE value is negative. It is worth noting that when measuring the extracted photocurrent at a certain applied potential and different light intensities, a stable record of the extracted photocurrent was obtained after 60 seconds of chronoamperometric measurement. However, for intensities below 10 mW cm^{-2}, and especially at the region below the OCP, the time

needed to reach a stable photocurrent value was around 120 s.

First, we carried out IMPS measurements at three different applied potentials and maximum illumination. In **Figure 2c**, at 0.45 V vs RHE, the IMPS signal at low frequency is clearly located at the positive real axis of the spectrum. At 0.25 V vs RHE, the IMPS response tends to zero at low frequency as shown in the zoom from **Figure 2d**, in good agreement with the evolution of the $\overline{J_e} - \overline{J_\phi}$ plot shown in **Figure 2b**, where a constant photocurrent is shown. Thus, we have

$$Q(0) = EQE_{diff} = 0 \tag{7}$$

Finally, at -0.05 V vs RHE, at the lowest frequency values, the IMPS transfer function moves to the negative part of the real axis, resulting in a negative $Q(0)$.

However, these measurements at maximum illumination, (i.e. at the points on the right side of **Figure 2b**) are not able to discriminate whether the IMPS sign switching is due to the photocurrent sign switching or to the EQE_{diff} one. Nevertheless, from the points at -0.05 V vs RHE in **Figure 2b**, we can differentiate two regions, one with negative photocurrent and negative slope (right side) and one with positive photocurrent and negative slope (left side), at lower illumination intensities. At this second region, the slope is negative and consequently, the differential EQE is also negative, even when the photocurrent is positive. This point allows clearly discriminating whether the IMPS sign is related to photocurrent sign, or to the sign of the slope of $\overline{J_e} - \overline{J_\phi}$ plot, i.e., the EQE_{diff}. If the IMPS switching is only related to the photocurrent switching, this point will give a positive $Q(0)$, whereas if IMPS is related to the EQE_{diff}, $Q(0)$ will be negative.

To better illustrate this, **Figure 3a** represents both the extracted photocurrent and the EQE_{diff} calculated from the slope of **Figure 2b**. Here it is shown unequivocally that, at the low illumination intensity region, the net extracted current is positive, while the slope is negative. At this point (same illumination intensity and applied voltage) we carried out IMPS measurements and found out that the IMPS transfer function at low frequency is also negative (**Figure 3b**), discarding the hypothesis that IMPS sign switching is related to photocurrent sign switching. At higher illumination intensities, the photocurrent is negative and, as shown before, the IMPS spectrum at the lowest frequency region is also negative (**Figure 3c**). Here, the negative IMPS is not related to the negative sign of the photocurrent, but its negative slope with increasing illumination.

Finally, we compared the values of the EQE_{diff} calculated from the slope of the data at -0.05 V vs RHE in **Figure 2b** with the values of $Q(0)$ extracted from IMPS spectra by extrapolating the final arc. As we expected, the values are in the same order of magnitude. The values are shown in **Table S1, in the Supporting Information**.

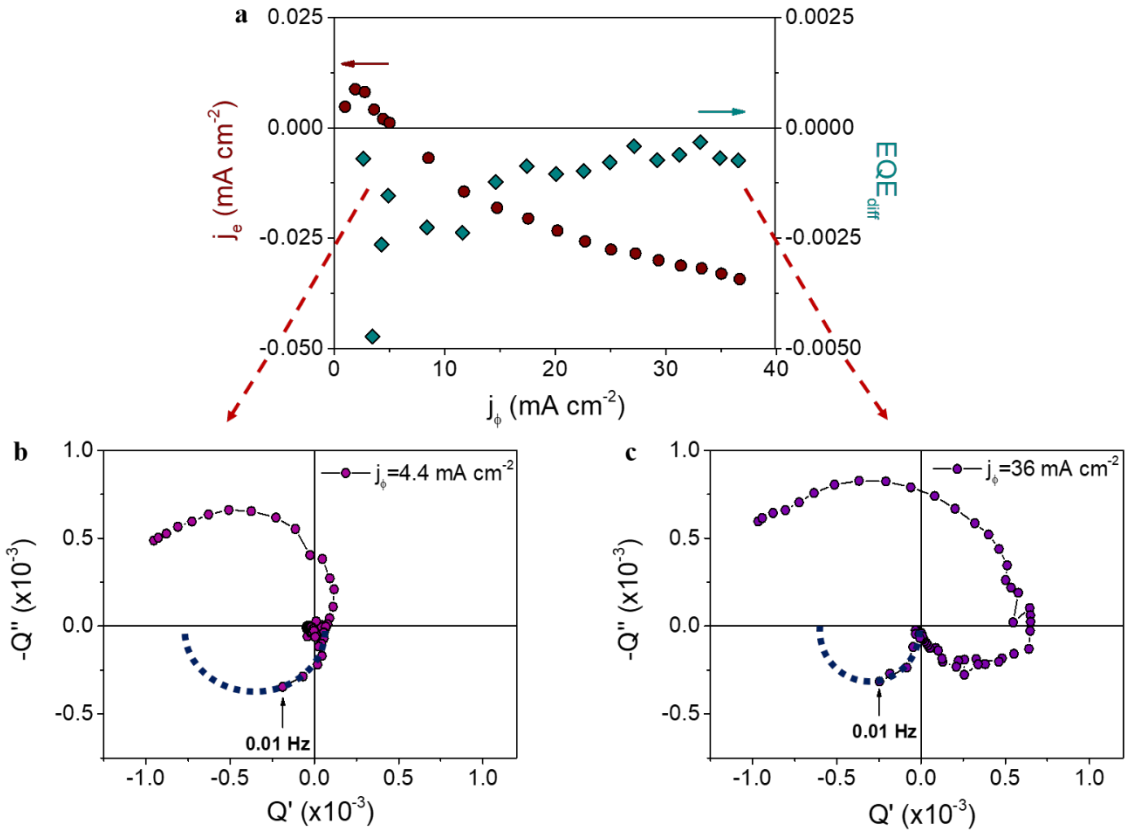

Figure 3. a Extracted photocurrent measured at -0.05 V vs RHE and EQE_{diff} calculated from the slope of steady-state values as function of the illumination intensity; **b** and **c** Q complex representation recorded under 4.4 mA cm^{-2} and 36 mA cm^{-2} photon current density, respectively, showing the tendency to negative values of the real part of Q at low frequency. We have included an extrapolation of the last arc to estimate the value of $Q(0)$.

The results discussed so far provide a general opto-electrical method of investigation of PEC cells that can yield a rich amount of information regarding its operation. The evolution of the steady state photocurrent with light intensity can provide direct intuition regarding specific recombination mechanisms, such as changes in ideality factors, trapping effects and injection barriers. For example, an EQE_{diff} value of 0 at voltages close to OCP as seen in Figure 1b (0.25 V vs RHE) indicates an invariant value of photocurrent for different light intensities, indicating that LSV measurements at different light intensities will converge to the same or very similar OCP value. This can indicate the occurrence of Fermi level pinning in the BVO_4 (as has been suggested from IS measurements in ref. [29]), where the applied potential is absorbed by a dipole at the interface, as has also been observed for crystal-deficient rutile TiO_2 nanowires[30]. For observations of a negative EQE_{diff} at voltages close to or beyond the OCP, it is likely that the applied light intensity promotes the filling of a local density of shallow traps around the electron Fermi level. This promotes recombination of the photogenerated

holes with the trapped electrons which, coupled with the poor transport properties of the $BiVO_4$, creates a reduction in the extracted photocurrent. Finally, for large reverse biases, the shallow traps are filled with holes, allowing the photogenerated holes to be extracted efficiently and causing a rise in photocurrent with light intensity.[31] Detailed validation of these mechanisms related to the negative EQE_{diff} is currently in progress but beyond the scope of the present Viewpoint.

In summary, we have experimentally demonstrated that the negative value of the real part of the transfer function observed in IMPS measurements is not a consequence of a current sign switching but indicating the change in the extracted photocurrent with a change in the incident photon flux intensity. We confirm this in $BiVO_4$ photoanodes by identifying a region beyond the OCP that shows a positive photocurrent while yielding a negative EQE_{diff} value. We also establish the study of photocurrent-light intensity spectra at different voltages as a powerful method to provide extra insight regarding specific mechanisms of operation such as trapping and recombination, and Fermi level pinning in PEC devices.

Drialys Cardenas-Morcoso
Agustín Bou
Sandheep Ravishankar
Miguel García-Tecedor
Sixto Gimenez*
Juan Bisquert*
Institute of Advanced Materials (INAM), Universitat Jaume I, 12006 Castelló, Spain

SUPPORTING INFORMATION

The Supporting Information is available free of charge on the ACS Publications website at DOI: xxx

Experimental details of photoelectrodes preparation, as well as equipment and conditions used for photoelectrochemical measurements. Table with differential quantum efficiency values extracted from IMPS and steady-state measurements (PDF)

AUTHOR INFORMATION

Corresponding Authors
*Email: sjulia@uji.es (S.G.)
*Email: bisquert@uji.es (J.B.)

ORCID

Notes

Views expressed in this Viewpoint are those of the authors and not necessarily the views of the ACS.

The authors declare no competing financial interest.

ACKNOWLEDGMENTS

We would like to acknowledge financial support from the Ministerio de Ciencia, Innovación y Universidades of Spain (ENE2017-85087-C3-1-R).

REFERENCES

1. Ravishankar, S.; Riquelme, A.; Sarkar, S. K.; Garcia-Batlle, M.; Garcia-Belmonte, G.; Bisquert, J. Intensity-Modulated Photocurrent Spectroscopy and Its Application to Perovskite Solar Cells. *The Journal of Physical Chemistry C* **2019,** *123* (41), 24995-25014.

2. Schneider, I. A.; Bayer, M. H.; Wokaun, A.; Scherer, G. G. Negative Resistance Values in Locally Resolved Impedance Spectra of Polymer Electrolyte Fuel Cells. *ECS Transactions* **2009,** *25* (1), 937-948.

3. Mora-Seró, I.; Bisquert, J.; Fabregat-Santiago, F.; Garcia-Belmonte, G.; Zoppi, G.; Durose, K.; Proskuryakov, Y. Y.; Oja, I.; Belaidi, A.; Dittrich, T.; Tena-Zaera, R.; Katty, A.; Lévy-Clement, C.; Barrioz, V.; Irvine, S. J. C. Implications of the negative capacitance observed at forward bias in nanocomposite and polycrystalline solar cells. *Nano Letters* **2006,** *6*, 640-650.

4. Fabregat-Santiago, F.; Kulbak, M.; Zohar, A.; Vallés-Pelarda, M.; Hodes, G.; Cahen, D.; Mora-Seró, I. Deleterious Effect of Negative Capacitance on the Performance of Halide Perovskite Solar Cells. *ACS Energy Letters* **2017,** *2* (9), 2007-2013.

5. Guerrero, A.; Garcia-Belmonte, G.; Mora-Sero, I.; Bisquert, J.; Kang, Y. S.; Jacobsson, T. J.; Correa-Baena, J.-P.; Hagfeldt, A. Properties of Contact and Bulk Impedances in Hybrid Lead Halide Perovskite Solar Cells Including Inductive Loop Elements. *The Journal of Physical Chemistry C* **2016,** *120* (15), 8023-8032.

6. Moia, D.; Gelmetti, I.; Calado, P.; Fisher, W.; Stringer, M.; Game, O.; Hu, Y.; Docampo, P.; Lidzey, D.; Palomares, E.; Nelson, J.; Barnes, P. R. F. Ionic-to-electronic current amplification in hybrid perovskite solar cells: ionically gated transistor-interface circuit model explains hysteresis and impedance of mixed conducting devices. *Energy & Environmental Science* **2019,** *12* (4), 1296-1308.

7. Ebadi, F.; Taghavinia, N.; Mohammadpour, R.; Hagfeldt, A.; Tress, W. Origin of apparent light-enhanced and negative capacitance in perovskite solar cells. *Nature Communications* **2019,** *10* (1), 1574.

8. Ghahremanirad, E.; Bou, A.; Olyaee, S.; Bisquert, J. Inductive Loop in the

Impedance Response of Perovskite Solar Cells Explained by Surface Polarization Model. *The Journal of Physical Chemistry Letters* **2017,** *8* (7), 1402-1406.

9. Klotz, D. Negative capacitance or inductive loop? – A general assessment of a common low frequency impedance feature. *Electrochemistry Communications* **2019,** *98*, 58-62.

10. Peter, L. M.; Wijayantha, K. G. U.; Tahir, A. A. Kinetics of light-driven oxygen evolution at α-Fe2O3 electrodes. *Faraday Discussions* **2012,** *155* (0), 309-322.

11. Dunn, H. K.; Feckl, J. M.; Müller, A.; Fattakhova-Rohlfing, D.; Morehead, S. G.; Roos, J.; Peter, L. M.; Scheu, C.; Bein, T. Tin doping speeds up hole transfer during light-driven water oxidation at hematite photoanodes. *Physical Chemistry Chemical Physics* **2014,** *16* (44), 24610-24620.

12. Thorne, J. E.; Jang, J.-W.; Liu, E. Y.; Wang, D. Understanding the origin of photoelectrode performance enhancement by probing surface kinetics. *Chemical Science* **2016,** *7* (5), 3347-3354.

13. Rodríguez-Pérez, M.; Rodríguez-Gutiérrez, I.; Vega-Poot, A.; García-Rodríguez, R.; Rodríguez-Gattorno, G.; Oskam, G. Charge transfer and recombination kinetics at WO3 for photoelectrochemical water oxidation. *Electrochimica Acta* **2017,** *258*, 900-908.

14. Thorne, J. E.; Zhao, Y.; He, D.; Fan, S.; Vanka, S.; Mi, Z.; Wang, D. Understanding the role of co-catalysts on silicon photocathodes using intensity modulated photocurrent spectroscopy. *Physical Chemistry Chemical Physics* **2017,** *19* (43), 29653-29659.

15. Zachäus, C.; Abdi, F. F.; Peter, L. M.; van de Krol, R. Photocurrent of BiVO4 is limited by surface recombination, not surface catalysis. *Chemical Science* **2017,** *8* (5), 3712-3719.

16. Liu, Y.; Le Formal, F.; Boudoire, F.; Yao, L.; Sivula, K.; Guijarro, N. Insights into the interfacial carrier behaviour of copper ferrite (CuFe2O4) photoanodes for solar water oxidation. *Journal of Materials Chemistry A* **2019,** *7* (4), 1669-1677.

17. Rodríguez-Gutiérrez, I.; Djatoubai, E.; Rodríguez-Pérez, M.; Su, J.; Rodríguez-Gattorno, G.; Vayssieres, L.; Oskam, G. Photoelectrochemical water oxidation at FTO|WO3@CuWO4 and FTO|WO3@CuWO4|BiVO4 heterojunction systems: An IMPS analysis. *Electrochimica Acta* **2019,** *308*, 317-327.

18. García-Tecedor, M.; Cardenas-Morcoso, D.; Fernández-Climent, R.; Giménez, S. The Role of Underlayers and Overlayers in Thin Film BiVO4 Photoanodes for Solar Water Splitting. *Advanced Materials Interfaces* **2019,** *6* (15), 1900299.

19. Kim, J. H.; Lee, J. S. Elaborately Modified BiVO4 Photoanodes for Solar Water Splitting. *Advanced Materials* **2019,** *31* (20), 1806938.

20. Tayebi, M.; Lee, B.-K. Recent advances in BiVO4 semiconductor materials for hydrogen production using photoelectrochemical water splitting. *Renewable and Sustainable Energy Reviews* **2019,** *111*, 332-343.

21. Zhong, D. K.; Choi, S.; Gamelin, D. R. Near-Complete Suppression of Surface Recombination in Solar Photoelectrolysis by "Co-Pi" Catalyst-Modified W:BiVO4. *Journal of the American Chemical Society* **2011,** *133* (45), 18370-18377.

22. Nellist, M. R.; Qiu, J.; Laskowski, F. A. L.; Toma, F. M.; Boettcher, S. W. Potential-Sensing Electrochemical AFM Shows CoPi as a Hole Collector and Oxygen Evolution Catalyst on BiVO4 Water-Splitting Photoanodes. *ACS Energy Letters* **2018,** *3* (9), 2286-2291.

23. Antuch, M.; Millet, P.; Iwase, A.; Kudo, A. The role of surface states during photocurrent switching: Intensity modulated photocurrent spectroscopy analysis of BiVO4 photoelectrodes. *Applied Catalysis B: Environmental* **2018,** *237*, 401-408.

24. Rodríguez-Gutiérrez, I.; García-Rodríguez, R.; Rodríguez-Pérez, M.; Vega-Poot, A.; Rodríguez Gattorno, G.; Parkinson, B. A.; Oskam, G. Charge Transfer and Recombination Dynamics at Inkjet-Printed CuBi2O4 Electrodes for Photoelectrochemical Water Splitting. *The Journal of Physical Chemistry C* **2018,** *122* (48), 27169-27179.

25. Miethe, J. F.; Lübkemann, F.; Poppe, J.; Steinbach, F.; Dorfs, D.; Bigall, N. C. Spectroelectrochemical Investigation of the Charge Carrier Kinetics of Gold-Decorated Cadmium Chalcogenide Nanorods. *ChemElectroChem* **2018,** *5* (1), 175-186.

26. Bertoluzzi, L.; Bisquert, J. Investigating the Consistency of Models for Water Splitting Systems by Light and Voltage Modulated Techniques. *The Journal of Physical Chemistry Letters* **2017,** *8* (1), 172-180.

27. Klotz, D.; Ellis, D. S.; Dotan, H.; Rothschild, A. Empirical in operando analysis of the charge carrier dynamics in hematite photoanodes by PEIS, IMPS and IMVS. *Physical Chemistry Chemical Physics* **2016,** *18* (34), 23438-23457.

28. Ravishankar, S.; Aranda, C.; Boix, P. P.; Anta, J. A.; Bisquert, J.; Garcia-Belmonte, G. Effects of Frequency Dependence of the External Quantum Efficiency of Perovskite Solar Cells. *The Journal of Physical Chemistry Letters* **2018,** *9* (11), 3099-3104.

29. Trześniewski, B. J.; Digdaya, I. A.; Nagaki, T.; Ravishankar, S.; Herraiz-Cardona, I.; Vermaas, D. A.; Longo, A.; Gimenez, S.; Smith, W. A. Near-complete suppression of surface losses and total internal quantum efficiency in BiVO4 photoanodes. *Energy & Environmental Science* **2017,** *10* (6), 1517-1529.

30. Zhang, K.; Ravishankar, S.; Ma, M.; Veerappan, G.; Bisquert, J.; Fabregat-Santiago, F.; Park, J. H. Overcoming Charge Collection Limitation at Solid/Liquid

Interface by a Controllable Crystal Deficient Overlayer. *Advanced Energy Materials* **2017,** *7* (3), 1600923.

31. Kelly, J. J.; Memming, R. The Influence of Surface Recombination and Trapping on the Cathodic Photocurrent at p- Type III- V Electrodes. *Journal of The Electrochemical Society* **1982,** *129* (4), 730-738.